frontiers | Frontiers in Materials

TYPE Original Research
PUBLISHED 02 November 2023
DOI 10.3389/fmats.2023.1292098

Check for updates

OPEN ACCESS

EDITED BY
Yan Huang,
Brunel University London,
United Kingdom

REVIEWED BY
Hua Men,
Brunel University London,
United Kingdom
Gang Li,
Soochow University, China

*CORRESPONDENCE
Xiaojie Li,
albertlxj@126.com
Junjie Du,
dujunjie205@hotmail.com

†These authors have contributed equally to this work and share first authorship

RECEIVED 11 September 2023
ACCEPTED 23 October 2023
PUBLISHED 02 November 2023

CITATION
Xie B, Yang F, Chen H, Zhang H, Ma H, Li T, Chen Z, Li J, Li X and Du J (2023), Electrospun polycaprolactone/silk fibroin nanofiber scaffold with aligned fiber orientation for articular chondrocyte regeneration. *Front. Mater.* 10:1292098. doi: 10.3389/fmats.2023.1292098

COPYRIGHT
© 2023 Xie, Yang, Chen, Zhang, Ma, Li, Chen, Li, Li and Du. This is an open-access article distributed under the terms of the Creative Commons Attribution License (CC BY). The use, distribution or reproduction in other forums is permitted, provided the original author(s) and the copyright owner(s) are credited and that the original publication in this journal is cited, in accordance with accepted academic practice. No use, distribution or reproduction is permitted which does not comply with these terms.

Electrospun polycaprolactone/silk fibroin nanofiber scaffold with aligned fiber orientation for articular chondrocyte regeneration

Bowen Xie[1,2†], Fengyuan Yang[1,3†], Hongguang Chen[4†], Hongxing Zhang[1,2†], Hebin Ma[4], Tianqi Li[1,3], Zhiqiang Chen[1,3], Jingyuan Li[1,2], Xiaojie Li[1*] and Junjie Du[1,2,3*]

[1]Fifth School of Clinical Medicine, Air Force Clinical College, Anhui Medical University, Hefei, China, [2]Department of Orthopedics, Air Force Medical Center of the PLA, Beijing, China, [3]Graduate School of Medicine, China Medical University, Shenyang, China, [4]Senior Department of Orthopedics, The Fourth Medical Center of the PLA General Hospital, Beijing, China

Objective: Electrospun nanofibers exhibit potential as scaffolds for articular cartilage tissue regeneration. This study aimed to fabricate electrospun polycaprolactone (PCL)/silk fibroin (SF) composite nanofiber scaffolds and to explore performance of the scaffolds for articular chondrocyte regeneration.

Methods: By altering material composition and preparation methods, three types of nanofiber scaffolds were effectively fabricated, including randomly oriented PCL (RPCL) nanofiber scaffold, randomly oriented PCL/SF (RPCL/SF) nanofiber scaffold, and aligned PCL/SF (APCL/SF) nanofiber scaffold. Physiochemical analyses were performed to determine mechanical properties and surface hydrophilicity of the nanofiber scaffolds. *In vitro* studies were conducted to investigate performance of the scaffolds on articular chondrocyte proliferation, gene expression and glycosaminoglycan secretion. Cytoskeleton staining was used to observe the arrangement of chondrocytes along the direction of the fibers and their elongation along the fiber arrangement.

Results: The physicochemical analysis demonstrated that the APCL/SF nanofiber scaffold exhibited improved mechanical properties and surface hydrophilicity compared to the RPCL and RPCL/SF nanofiber scaffolds. Furthermore, the *in vitro* cell culture studies confirmed that the APCL/SF nanofibers could significantly promote articular chondrocyte proliferation, type II collagen (*COL-II*) gene expression, and glycosaminoglycan secretion compared to the RPCL and RPCL/SF nanofiber scaffolds. Additionally, cytoskeletal staining displayed that the APCL/SF nanofiber scaffold promoted the elongation of articular chondrocytes in the direction of parallel fiber alignment.

Conclusion: The APCL/SF nanofiber scaffold exhibited promising potential as a composite scaffold for articular cartilage regeneration.

KEYWORDS

polycaprolactone, silk fibroin, electrospinning, surface morphology, material orientation, articular chondrocyte, articular cartilage regeneration

1 Introduction

Articular cartilage lacks blood vessels, nerves, and lymphatic tissue. Once damaged, its ability to self-repair and regenerate is severely limited (Armiento et al., 2019). Therefore, the progressive degeneration of the articular cartilage is an irreversible injury, which can lead to osteoarthritis (OA) impacting the patient's daily life (Makris et al., 2015). Current treatment options for cartilage injuries include microfracture surgery (Redondo et al., 2018), autologous chondrocyte transplantation (Na et al., 2019), and allogeneic or autologous cartilage transplantation (Gao et al., 2019; Christensen et al., 2021). While these treatments may enhance joint function and alleviate pain to a certain degree, they frequently result in chondrofibrosis. Furthermore, issues such as donor shortage, poor integration, and surgical infections severely limit their extensive application (Zhou et al., 2023). Subsequently, the complex nature of articular cartilage injuries and the limited treatment alternatives make it one of the most challenging clinical issues in orthopedics (Johnstone et al., 2013; Makris et al., 2015).

Cartilage tissue engineering, an approach that combines functional cells, suitable materials, and biochemical cues in specifically designed scaffolds, is a highly effective and promising method for treating damage to articular cartilage (Kai et al., 2011b). The bioscaffolds function as interim substitutes for the extracellular matrix (ECM), as they duplicate the advantageous properties of the natural ECM, providing a three-dimensional (3D) structure for engineered tissues. Furthermore, the bioscaffolds can serve as a structural support and provide metabolic sites for cell adhesion, proliferation, and differentiation, ultimately leading to tissue regeneration. The selection of bioscaffold materials is critical for the success of cartilage tissue engineering, and each category of materials presents unique advantages and disadvantages that must be considered.

Polycaprolactone (PCL) is commonly utilized in tissue engineering for its safety, nontoxicity, good biodegradability, mechanical properties, biocompatibility, and easy availability of raw materials. Recent studies have shown promising results in treating bone, cartilage, and flat bone defects with PCL (Malikmammadov et al., 2018; Saracino et al., 2021). Silk fibroin (SF) is a protein polymer with desirable properties, such as hydrophilicity, biodegradability, and low immunogenicity, for material formation (Xie et al., 2019). SF also possesses ligands, like arginine-glycine-aspartic acid (RGD) motifs, that facilitate cell adhesion, migration, and proliferation (Min et al., 2004; Li et al., 2011). As a natural material, SF has significant potential for use in skin, nerve, bone, and cartilage tissue engineering (Li et al., 2015; Farokhi et al., 2018). However, PCL and SF both have limitations as scaffold materials in tissue engineering. The inherent hydrophobicity and lack of cell affinity in PCL, caused by the absence of recognition sites for cell adhesion, limit its application in biomedical fields with PCL nanofiber scaffolds (Lee et al., 2011; Liao et al., 2012; Yang et al., 2023). Pure SF electrospun yarn has poor mechanical properties and ductility, which hinders its use in tissue engineering (Ki et al., 2009).

It appears that only composite scaffolds can fulfill the ideal comprehensive properties that cannot be achieved by a single material. In recent decades, significant strides have been made in researching composite cartilaginous scaffolds comprising natural and synthetic polymer materials due to their machinability and mechanical properties (Torricelli et al., 2014; Silva et al., 2020; Zhao et al., 2020). However, its physiological structure and biomechanical properties differ greatly from those of natural cartilage, the biocompatibility, *in vivo* stability, fatigue resistance and flexibility of the material still restrict its research, development, and application (Zelinka et al., 2022). Critchley et al. (Critchley et al., 2020) designed bi-phasic 3D printed scaffolds for the treatment of osteochondral defects. The scaffolds contained MSCs-containing hydrogels as the 'osseous phase' below, while a self-assembled MSC-chondrocyte layer acted as the 'chondral phase' on top. This example highlights the design of 3D printed cell-seeded scaffolds for osteochondral regeneration. However, the 3D-printed matrix scaffolds encounter significant problems. For instance, the resolution limitations of 3D printing hinder the construction of scaffolds' nanostructure. Additionally, various 3D-printed scaffolds' mechanical properties do not measure up to those of host tissues (Xue et al., 2023). Compared to 3D printing and other traditional methods, electrospinning technique is a more effective and advantageous method to control the final unique structures and properties of scaffolds (Jun et al., 2018). Electrospun films provide several advantages, such as high surface area-to-volume ratio, porosity, and easy modification (Casanova et al., 2018). Additionally, they can mimic the fibrous arrangement present in the natural ECM of cartilage tissue, fuse closely with cells, and provide nutritional support (Zhou et al., 2018). Thus, the produced nanofiber film may exhibit good mechanical properties and biocompatibility, fulfilling requirements of composite materials for cartilage tissue engineering (Chen et al., 2017; Cheng et al., 2017). Notably, the electrospinning technique allows the fabrication of nanofiber scaffolds with random and aligned orientations (Li et al., 2015), which significantly affects the orientation and function of cell adhesion (Kai et al., 2011b).

To address the limitations of using either PCL or SF alone, it was proposed to electrospin PCL and SF in a certain ratio. This enables both materials to integrate the desired properties of PCL and SF into electrospun films. While previous studies have utilized PCL and SF as bioscaffold materials for engineering skin, bone, nerve, ligament, and tendon artificial implants (Li et al., 2015; Steffi et al., 2018; Saremi et al., 2021), they have ignored the effect of material surface topography on cell growth, proliferation, and morphology, especially in chondrocytes. Further exploration is necessary to determine the potential of PCL composite SF nanofiber scaffolds in cartilage tissue engineering, with a particular focus on the effect of nanofiber orientation on chondrocyte growth, proliferation, and morphology.

Based on the promising potential for cartilage regeneration using PCL and SF, our study will fabricate novel composite scaffolds doped with PCL and SF by electrospinning technique and treated with nanofibrous orientation modification. The surface topographies and hydrophilicity, mechanical properties and biocompatibility of the scaffolds will be determined to compare the different material composition and nanofiber orientation for articular chondrocyte regeneration.

2 Materials and methods

2.1 Materials preparation

2.1.1 Extraction of silk fibroin (SF)

Bombyx mori (Northwest Sericulture Base, China) cocoons were degummed and processed to obtain SF according to the method described in a previous study (Rockwood et al., 2011). The mulberry

cocoons were boiled in a 0.02 mol/L Na_2CO_3 solution for 30 min. Stirring with a glass rod continuously facilitated degumming. After, they were washed three times with water and dried overnight in a 37°C thermostat. The degummed and dried silk was then dissolved in a 9.3 mol/L lithium bromide (LiBr) solution at 60°C for 4 h. The completely dissolved silk solution was then centrifuged at high speed to remove impurities, filtered, and dialyzed at room temperature for 3 days. Deionized water was changed every 6 h. This solution was frozen overnight in a −20°C refrigerator and then freeze-dried for 2 days to obtain spongy silk protein.

2.1.2 Fabrication of nanofiber scaffolds by electrospinning

To prepare randomly oriented PCL (RPCL) nanofiber scaffolds, 2 g of PCL (Shanghai Maclean's Reagent, China) with an average molecular weight of 80,000 Da was accurately weighed using an electronic balance and then dissolved in 10 mL of hexafluoroisopropanol (Shanghai Aladdin Biochemical Technology, China) solution to form a mixed electrospinning solution containing 20% PCL. 2 g of PCL and 0.4 g of SF were accurately weighed and then stirred in a magnetic stirrer at a ratio of 5:1 for 4 h until complete dissolution. This produced a homogeneous co-blended spinning solution for preparation of RPCL/SF and APCL/SF nanofiber scaffolds.

To prepare RPCL nanofibers, the electrostatic spinning solution was drawn into a syringe using a blunt 21G needle. The syringe was then mounted on an electrospinning machine (Yongkang Leye Technology Development Co., Beijing, China) before being pushed at a rate of 0.3 mm/min. The distance between the needle tip and the receiver (roller) was adjusted to 10 cm. Positively charged high voltage of 15 kV was applied to the syringe needle end, while negatively charged high voltage of −1 kV was applied to the receiver end. An aluminum foil-covered receiver device, rotating at a speed of 300 rpm/min, was utilized to accumulate the RPCL nanofibers. Similar procedures were followed for RPCL/SF nanofiber scaffolds. But for APCL/SF nanofibers, the receiver device rotated at a high speed of 5000 rpm and was also covered with aluminum foil. To maintain material integrity, two tubes of 10 mL electrospinning solution were sprayed on each nanofiber. After completing the electrospinning process, the electrospun film was removed and then vacuum-treated in a vacuum drying oven at 40°C for 48 h to remove hexafluoroisopropanol. The electrospun nanofiber scaffolds were then stored in a vacuum drying oven until further use.

2.2 Material characteristics

2.2.1 Scanning electron microscopy (SEM) analysis

The RPCL, RPCL/SF, and APCL/SF fibrous films that were prepared previously were cut into small, square pieces, each measuring 1 × 1 cm (n = 3). These pieces were then glued and fixed onto a 5 cm sample stage. After that, they were sprayed with gold, and the morphology of the nanofibers was observed using a SEM (E−1045, Hitachi, Japan), operating under 5 kV voltage and 10 μA current conditions. The average diameter and orientation of the nanofiber film were determined by using ImageJ software. All nanofiber orientation angles were measured relative to the defined vertical direction (0°).

2.2.2 Fourier-transform infrared spectroscopy (FTIR) analysis

RPCL and RPCL/SF nanofiber scaffolds were cut into small 1 × 1 cm squares to ensure a flat and smooth sample surface. These square samples were analyzed in the reaction chamber of an FTIR analyzer (Ettlingen, Germany). The analysis was carried out using absorption spectrometry within the range of 450 to 4,000 cm^{-1} at a resolution of 1 cm^{-1}. The functional groups found in the electrospun films were identified through the absorption peaks of infrared wavelengths, offering valuable insights into the composition of the nanofiber scaffolds.

2.2.3 Mechanical testing

The mechanical properties of the three nanofiber scaffolds were analyzed using a uniaxial tensile testing machine (Wanchen Testing Machine Co., Shandong, China). Samples of each nanofiber scaffold, measuring 10 × 20 mm^2 with a thickness of approximately 0.10 mm (n = 3), were prepared. Prior to testing, each sample was preloaded with 0.1 N to prevent relaxation. Then, the samples were stretched at a rate of 5 mm/min until fracture. The stress-strain curves were used to measure the tensile strength and elongation at break.

2.2.4 Contact angle test

Contact angle measurements were conducted to assess the electrospun nanofibers' hydrophilicity/hydrophobicity. The nanofiber scaffolds were cut into 1 × 1 cm pieces (n = 5), and deionized water was dropped onto the nanofiber surface using the static drop technique. The resulting droplet's profile image was captured using a microscope head camera (Dataphysics OCA20, Germany) from the side when 1 mL of distilled water was added to the samples, and photographs were taken after 1 s of contact. The tests were repeated five times and the results were averaged. The contact angle of the droplet's surface was calculated using digital image processing software provided with the computer.

2.3 *In vitro* cell experiments

2.3.1 Isolation and culture of rabbit knee cartilage

All animal experiments were approved by the Ethics Committee of Keyu Animal Breeding Center (Beijing, China). Two-week-old New Zealand rabbits were killed by means of air injections along the ear margins. Skin preparation for knee joint exposure. The knee joint's soft outer membrane tissue was peeled off on an ultra-clean table. Then, the synovial membrane that covers the cartilage surface was carefully removed, and the cartilage was cut into 1 mm^3 pieces with surgical scissors. These articular cartilage pieces were washed three times with a phosphate-buffered saline (PBS) solution and subjected to digestion with 0.2% type II collagenase at 37°C for approximately 10 h. The entire experiment was performed under aseptic conditions. The cell culture medium was changed every other day, and third-generation cells were utilized for subsequent experimental studies.

2.3.2 Cell proliferation

The RPCL, RPCL/SF and APCL/SF nanofiber scaffolds were cut into 10 mm diameter discs and sterilized by ultraviolet light irradiation for 2 h on both sides. Following that, they were

immersed in a 75% ethanol solution for 30 min and then washed three times with sterile PBS solution to remove the residual alcohol. The samples were placed in cell culture medium overnight and then inoculated with articular chondrocytes at a density of 1×10^4 cells/well. The articular chondrocytes were distributed into 48-well plates. This experiment was divided into three groups, with each group comprising four replicate wells. To culture the cells, 500 μL of DMEM/F-12 medium (Wuhan Doctoral Biological Engineering, China) supplemented with fetal bovine serum (Shanghai Dartheil Biotechnology, China) was added to each group. The cells were then incubated in a 5% CO_2 incubator at 37°C for 5 days. Additionally, 50 μL of Cell Counting Kit-8 (CCK-8) (Abmole, United States) reagent was added on days 1, 3, and 5, followed by incubation for 2 h. Absorbance (ABS) values were then measured at a wavelength of 450 nm.

2.3.3 Live/dead assay

Cell viability was evaluated using the live/dead cell staining kit (Beyotime Biotechnology Co., Shanghai, China). The staining process involved double fluorescence staining for both live and dead cells in a 48-well plate following the manufacturer's instructions. After being cultured up to day 5, the medium was removed and then washed three times with PBS. The scaffold-cell complex was immersed in a working solution containing calcein acetoxymethyl ester and propidium iodide reagents and incubated for 30 min at room temperature shielded from light. The adhesion and activity of articular chondrocytes on the different materials were observed by a fluorescent microscope.

2.3.4 Cytoskeletal staining with DAPI/F-actin

The chondrocytes were cultured for 3 days, and their attachment to the nanofiber surface was observed by actin staining. The material was washed with a PBS solution, fixed with 4% paraformaldehyde for 20 min, and then washed three times with PBS. Next, the nanofiber scaffold was treated with 0.1% Triton X-100 for 20 min and washed three times with PBS. The scaffold-cell complex was stained according to the kit instructions, and the cytoskeletal protein (F-actin) was stained with phalloidin, followed by DAPI staining solution to stain the nuclei. The observation of the staining was conducted under a fluorescent microscope.

2.3.5 Quantitative detection of DNA and sulphated GAG (sGAG) content

After chondrocyte inoculation in each scaffold group, they were cultured *in vitro* for 7 and 14 days. Then, the samples were digested with pre-prepared papain solution (125 mg/mL papain, 100 mM Na_2HPO_4, 5 mM EDTA, pH 6.4) at 60°C for 16 h. The DNA content of the samples was determined using the Qubit FlexTM instrument (Thermo Fisher Scientific, United States). The sGAG content was quantified using an sGAG assay kit (Jiubang Biotechnology, China). The sGAG and DNA contents of each scaffold group were determined, and the fibrocartilage matrix content was quantified by normalizing the DNA content.

2.3.6 Gene expression analysis

The RNA isolation and complementary DNA (cDNA) synthesis procedures were carried out in accordance with the kit instructions. Trizol (Tiangen Biotech, China) was employed to isolate RNA from chondrocytes, followed by scaffold disruption to collect the cell suspension. Total RNA was then converted to cDNA with a reverse transcription kit (Accurate Biotechnology, China). cDNA was extracted from chondrocytes using a real-time quantitative PCR detector (Applied Biosystems QuantStudio™ 7 Flex, United States) and a qPCR kit (Accurate Biotechnology, China). The qPCR conditions were as follows: 95°C for 3 min, followed by 40 cycles at 95°C for 10 s and 60°C for 30 s. Relative gene expression was calculated using the qPCR assay following the $2^{-\Delta\Delta CT}$ method (Schmittgen and Livak, 2008). Glyceraldehyde 3-phosphate dehydrogenase was used as an internal reference gene to analyze gene expression of collagen type II (*COL-II*), collagen type I (*COL-I*), aggregated protein (*ACAN*), and *SOX-9* (Guo et al., 2021).

2.4 Statistical analysis

One-way analysis of variance (ANOVA) was employed to compare multiple groups, followed by LSD test as a *post hoc* comparison. The quantitative data was presented as mean ± standard deviation (n = 3–5), with p-values < 0.05 were considered significant.

3 Results and discussion

3.1 The physicochemical characteristics of the nanofiber scaffolds

3.1.1 Morphological characteristics

The SEM analysis of RPCL, RPCL/SF, and APCL/SF samples was performed, and Figure 1A shows that no bead formation occurred in any of the three nanofiber films, and the fiber diameters were uniform. The RPCL and RPCL/SF scaffolds both featured randomly oriented nanofibers on their surfaces, whereas the APCL/SF scaffold exhibited a consistent unidirectional arrangement of nanofibers. Additionally, the SEM images revealed that all the three scaffolds exhibited a porous structure similar to that of natural cartilage ECM, which is necessary for the transport of nutrients and metabolic waste (Lowery et al., 2010; Li et al., 2016).

The orientation alignment of the nanofibers is shown in Figure 1B. The accompanying histogram depicts the alignment of nanofiber orientation in RPCL, RPCL/SF, and APCL/SF nanofiber scaffolds in relation to the vertical 0° line. The alignment of APCL/SF (8.6°) was significantly superior than RPCL (33.2°) and RPCL/SF (29.1°). The diameter of the nanofibers was displayed in Figure 1C. The diameter of RPCL nanofibers was around 552.4 ± 189.8 nm, with RPCL/SF measuring about 423.6 ± 199.4 nm and APCL/SF at approximately 361.9 ± 151.3 nm. No significant differences were detected in the average fiber diameter among the nanofiber films. The presence of SF in the solution may have led to a decrease in the nanofibers' average diameter, presumably resulting from the electrical conductivity of the blends increasing with SF content (Wang et al., 2021).

3.1.2 Material composition

FTIR analysis confirmed the presence of the PCL and SF composite (Figure 2A). The FTIR spectra of RPCL nanofibers

10.3389/fmats.2023.1292098

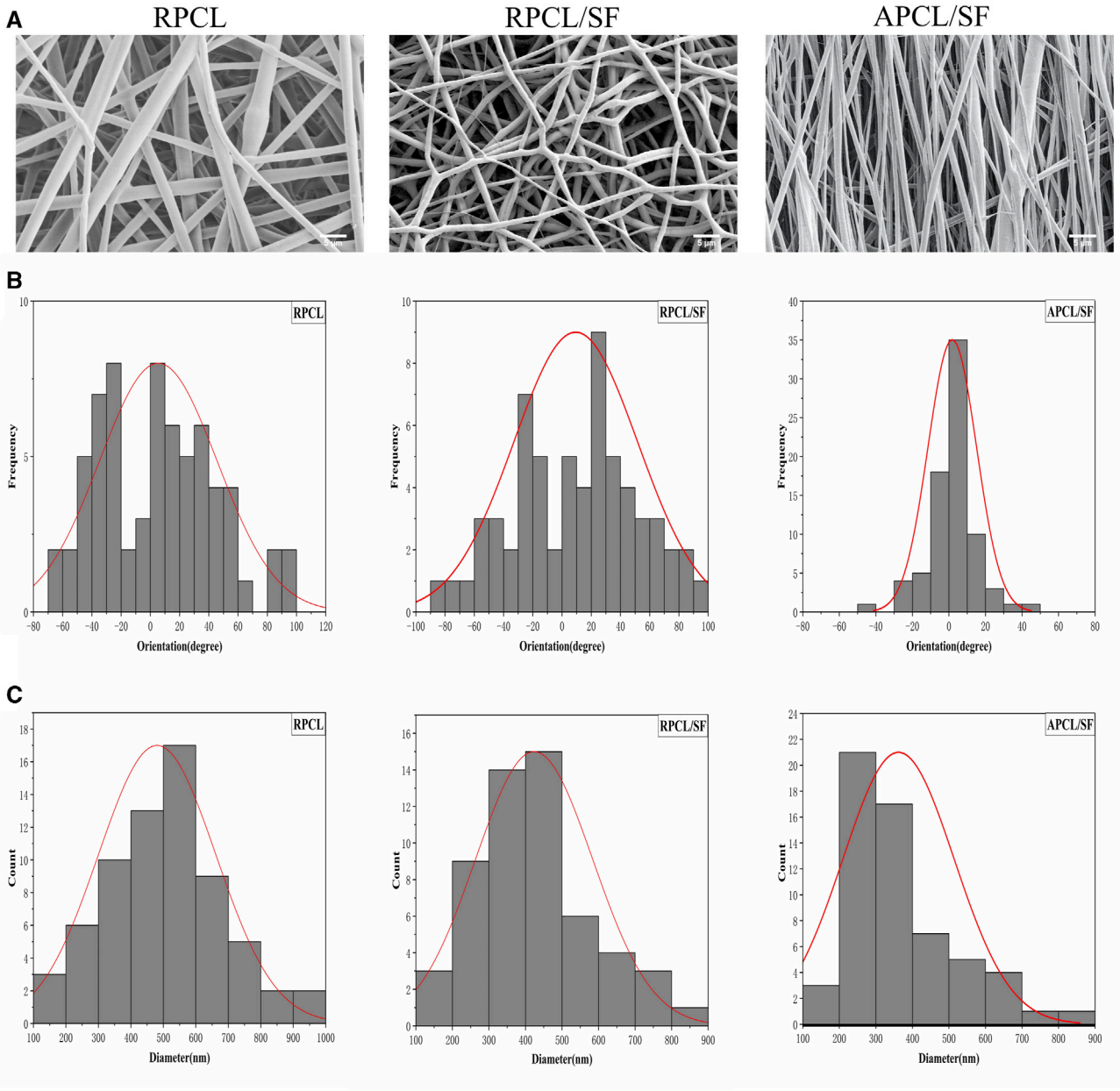

FIGURE 1
(A) Scanning electron microscopy (SEM) analysis for RPCL, RPCL/SF, and APCL/SF nanofiber scaffolds. **(B)** Nanofiber orientation. **(C)** Nanofiber diameter distribution.

showed distinctive peaks in the C-H stretching vibration range at 2947 cm^{-1} and 2867 cm^{-1}, as well as in the -C=O carbonyl ester stretching vibration range at 1722 cm^{-1}, indicating the presence of the PCL component (Li et al., 2011). Furthermore, the peaks at 1180 cm^{-1} and 1171 cm^{-1} suggest asymmetric C-O-C stretching and symmetric C-O-C stretching in PCL chains, respectively. The RPCL/SF nanofibers display noteworthy absorption peaks at 1655 cm^{-1} (amide I band) and 1542 cm^{-1} (amide II band), indicating the presence of SF in the form of random nematic clusters (Chen et al., 2017). The absorption peak at 1231 cm^{-1} (amide III band) is attributed to SF, which constitutes a complex band of C-N and N-H vibrational combinations, and coincides with the C-O-C asymmetric stretching band in PCL. Amide I and amide II constitute the primary bands of the SF structure (Roy et al., 2018).

3.1.3 Mechanical properties

Figure 2B and Table 1 demonstrate the effect of modifying nanofiber alignment and blending SF on the mechanical properties of PCL. The tensile strength of RPCL nanofibers was approximately 1.028 ± 0.062 MPa, while RPCL/SF measured around 4.046 ± 0.519 MPa and APCL/SF measured approximately 7.370 ± 2.238 MPa. The RPCL nanofibers' elongation at break was approximately 71.850 ± 0.156%, with RPCL/SF measuring about 20.300 ± 1.646% and APCL/SF at approximately 19.200 ± 2.858%.

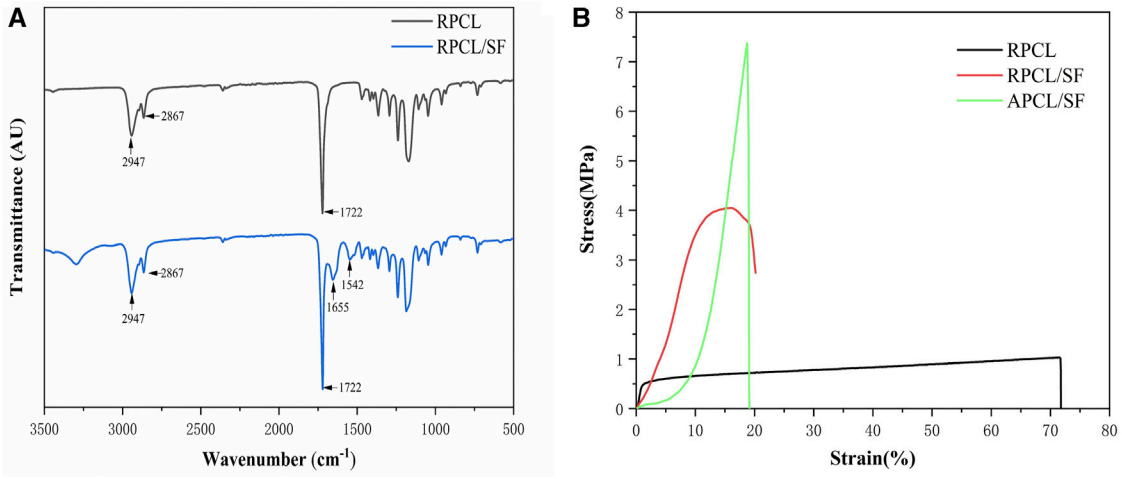

FIGURE 2
(A) Analysis of Fourier-transform infrared spectroscopy (FTIR) results for RPCL and RPCL/SF scaffold samples. **(B)** Tensile stress-strain curves for RPCL, RPCL/SF, and APCL/SF scaffold samples.

TABLE 1 Comparison of tensile properties of RPCL, RPCL/SF, and APCL/SF nanofiber scaffolds (mean ± standard deviation).

	RPCL	RPCL/SF	APCL/SF
Tensile strength (MPa)	1.028 ± 0.062	4.046 ± 0.519[a]	7.370 ± 2.238[a,b]
Elongation at break (%)	71.850 ± 0.156	20.300 ± 1.646[a]	19.200 ± 2.858[a]

[a]Compared with the RPCL group, $p < 0.05$.
[b]Compared with the RPCL/SF group, $p < 0.05$.

While the mechanical strength of APCL/SF was significantly higher than RPCL and RPCL/SF, RPCL's ductility was better than the other two groups.

Prior studies have shown that the strength of nanofiber films depends significantly on nanofiber orientation and electrostatic spinning components (Lee and Kim, 2010). PCL, being a thermoplastic polymer with good ductility, exhibits high elongation at break but relatively low mechanical strength in RPCL. SF has been demonstrated to possess excellent mechanical properties, particularly when obtained through degumming, a process that emphasizes retaining the protein structure of SF (Teh et al., 2010). As such, SF is appropriate for tissue engineering applications that necessitate high mechanical strength (Sahoo et al., 2010; Roy et al., 2018). The incorporation of SF enhanced the tensile strength of PCL, imparting adequate mechanical properties to the scaffolds to withstand shear forces within the cartilage tissue (Orash Mahmoud Salehi et al., 2020). This effect could be attributed to the ability of SF to increase the stiffness of the nanofibers and augment the structural integrity of the scaffold. However, previous studies have shown that pure SF has the lowest elongation at break and the weakest brittleness compared to pure PCL and PCL/SF, and exhibits rigid mechanical properties that do not allow it to be used alone as a synthetic cartilage scaffold (Yuan et al., 2016); therefore, pure SF scaffolds were not evaluated in this study. Additionally, the orientations of nanofiber scaffolds significantly affect the mechanical properties of electrostatically spun scaffolds. APCL/SF demonstrated nearly twice the tensile strength of RPCL/SF, as aligning the nanofibers resulted in a more uniform orientation and greater mechanical strength, with minimal impact on elongation at break. The mechanical properties of individual nanofibers and the resulting material may be affected by the random orientation of nanofiber films (Roy et al., 2018). Moreover, increasing nanofibers per unit volume enhances the mechanical strength of APCL/SF (Chen et al., 2017). Overall, the topographical features of the scaffold material greatly affect the mechanical properties of the scaffold.

3.1.4 Surface hydrophilicity

Surface hydrophilicity is a significant characteristic in biomaterials that impacts cell adhesion, proliferation, and migration. Figure 3 displays the hydrophilicity of the three groups of materials as determined by direct measurement of the water contact angle. Incorporating SF into RPCL caused the contact angle of RPCL/SF to fall from 130.5° to 90.3°. The contact angle of APCL/SF decreases to 62.5° compared to RPCL/SF when transitioning from randomly oriented to aligned oriented nanofibers. The hydrophilicity improves as the angle decreases (Qin et al., 2023). Therefore, RPCL held the worst surface hydrophilicity among the three groups, while APCL/SF had the best.

We hypothesize this improvement occurred due to the introduction of SF, which contains several hydrophilic groups, making RPCL/SF less hydrophilic than RPCL. This modification enhances cell adhesion to the material. Previous studies indicate that surface roughness creates a barrier effect, which impacts droplet expansion and increases the surface contact angle (Chung et al., 2007). The surface roughness of RPCL/SF restricts droplet spreading, while the smoother surface of APCL/SF aids droplet elongation, leading to a considerable decrease in contact angle (Kai et al., 2011a). In general, the scaffold material's topographical features have a great influence on the hydrophilicity of the scaffold.

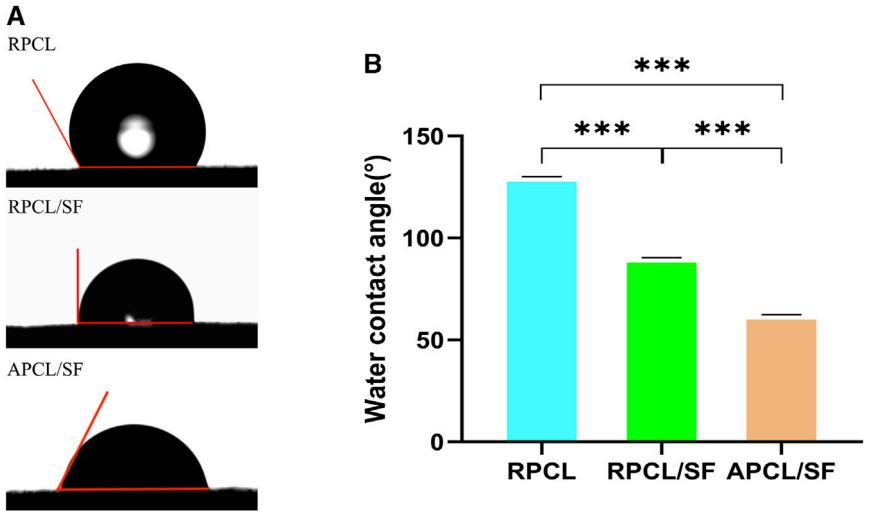

FIGURE 3
Images of water contact angles **(A)** and the corresponding histogram **(B)** of RPCL, RPCL/SF, and APCL/SF scaffold samples. Comparison between the two groups, ***$p < 0.001$.

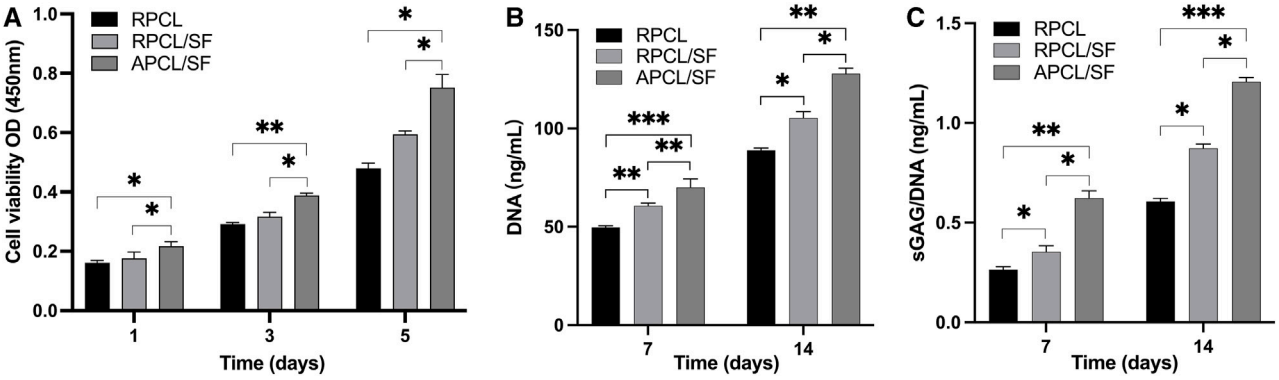

FIGURE 4
(A) The effect of RPCL, RPCL/SF, and APCL/SF nanofiber scaffolds on chondrocyte proliferation on days 1, 3 and 5. The DNA contents **(B)** and sGAG/DNA ratios **(C)** in RPCL, RPCL/SF, and APCL/SF groups on days 7 and 14. Comparison between the two groups, *$p < 0.05$, **$p < 0.01$, and ***$p < 0.001$.

3.2 The regeneration capacity of the nanofiber scaffolds for articular chondrocytes

Figure 4A displays the CCK-8 assay outcomes for optical density (OD) at different time points (days 1, 3, and 5) to compare cell proliferation in each material group. The relative cell count differences between the APCL/SF and RPCL groups were statistically significant on days 1, 3, and 5. The enhanced hydrophilic nature of the material may be linked to the proliferation of mesenchymal stem cells (MSCs), osteoblasts, and chondrocytes (Lampin et al., 1997; Zhang et al., 2009). The inclusion of SF may introduce bio-functional groups like -NH2- and -COOH, which could facilitate cell recognition and scaffolding, leading to increased cell proliferation (Faucheux et al., 2004). The number of cells within the APCL/SF group was consistently greater than the RPCL/SF group on days 1, 3, and 5, with a significant statistical difference. This may be related to the surface morphology of the material, as aligned oriented fibrous scaffolds may be able to promote cell proliferation more than randomly oriented fibrous scaffolds. The hydrophilic nature of the material surface promotes cell adhesion and may explain why the APCL/SF group exhibits greater cell proliferation than the RPCL and RPCL/SF groups. Taken together, the surface topography and chemical composition of biological scaffolds may influence cell growth.

Cell viability was evaluated on randomly oriented and aligned scaffolds using a live/dead staining assay. Figure 5A demonstrates the chondrocyte adhesion onto RPCL, RPCL/SF, and APCL/SF nanofiber scaffolds on day 3. Live cells (stained green) inoculated onto the RPCL and RPCL/SF scaffolds were randomly aligned and irregularly shaped. In contrast, live cells (stained green) inoculated with the APCL/SF scaffold were aligned in the same direction as the

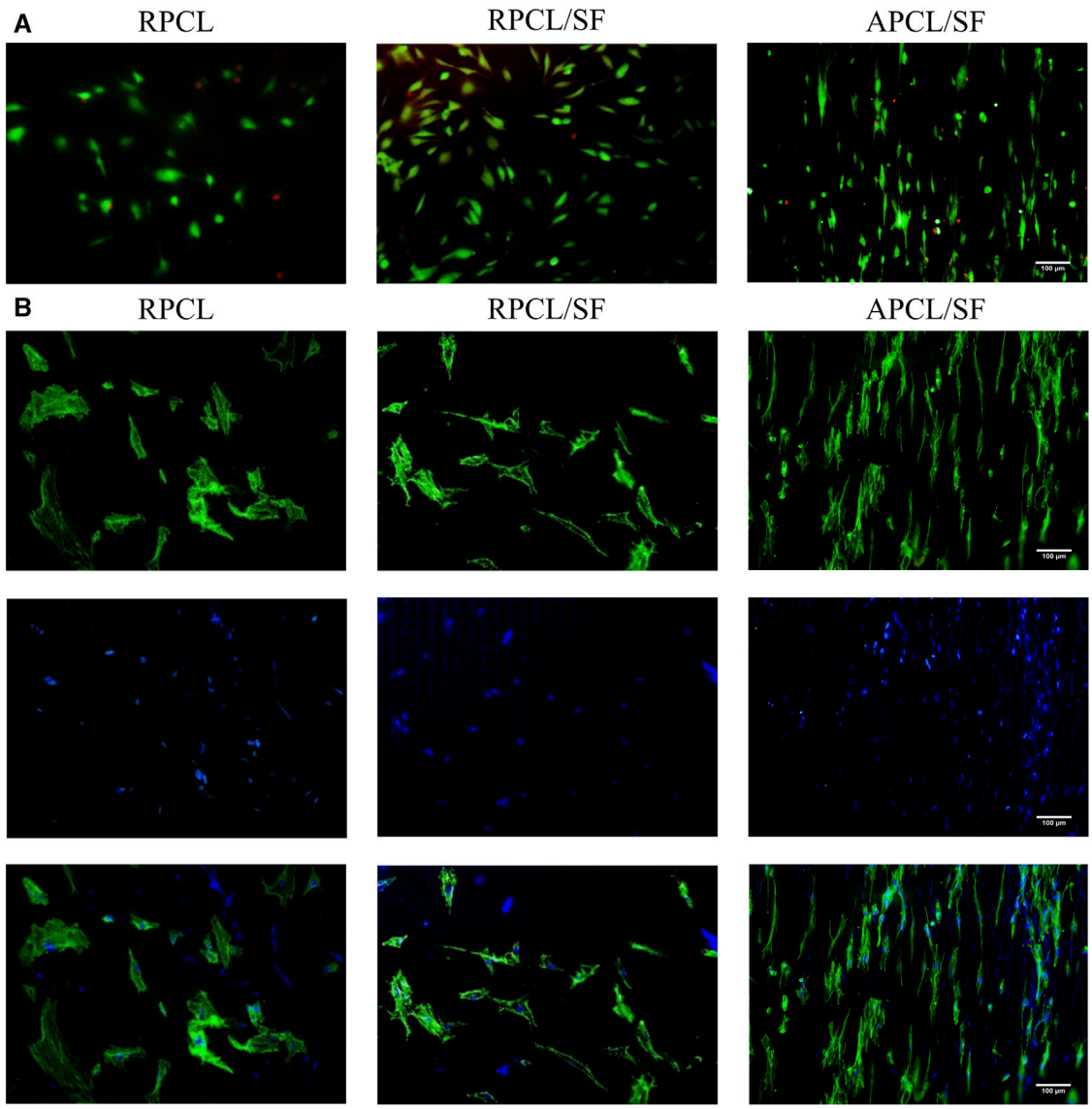

FIGURE 5
Results of live/dead staining **(A)** and DAPI/F-actin staining **(B)** of articular chondrocytes in RPCL, RPCL/SF, and APCL/SF groups on day 3.

nanofibers and exhibited a shuttle-like morphology. A small number of dead cells (stained red) were present in all three scaffolds, with a significant increase in cell density due to proliferation. On day 3, the number of dead cells was higher in the RPCL group as compared to the RPCL/SF and APCL/SF groups based on cell density observations. This finding is consistent with the results of the cell proliferation assay.

Chondrocyte growth and morphology on RPCL, RPCL/SF, and APCL/SF nanofiber scaffolds were examined through DAPI/F-actin staining. Figure 5B shows that a disordered actin cytoskeleton was observed on the surfaces of RPCL and RPCL/SF scaffolds on day 3.Cells cultured on the randomly oriented scaffolds showed polygonal structures with numerous filamentous pseudopods. Conversely, the actin cytoskeleton in APCL/SF was aligned parallel to the nanofiber axis, and the cells exhibited an elongated, shuttle-like shape along the direction of nanofiber alignment. When cells were topologically aligned along the direction of the nanofibers, nanofiber alignment had a significant impact on cell proliferation, orientation, and an increase in cartilage matrix content (Zhang et al., 2012). The DAPI/F-actin staining results demonstrated that the orientation of the material nanofibers influenced the directional growth of cells. The positive effects of aligned nanofibers on cell elongation and proliferation. Specifically, the APCL/SF scaffold enhanced chondrocyte proliferation and facilitated their stretch migration, demonstrating superiority to the RPCL and RPCL/SF constructs.

The ability of RPCL, RPCL/SF, and APCL/SF nanofiber scaffolds to promote chondrocytes to produce cartilage ECM was evaluated by quantifying the fibrocartilage matrix content normalized by DNA content and sGAG/DNA ratio. The outcomes of DNA contents and sGAG/DNA ratios are presented in Figures 4B, C. The DNA contents and sGAG/DNA ratios of chondrocytes on the three

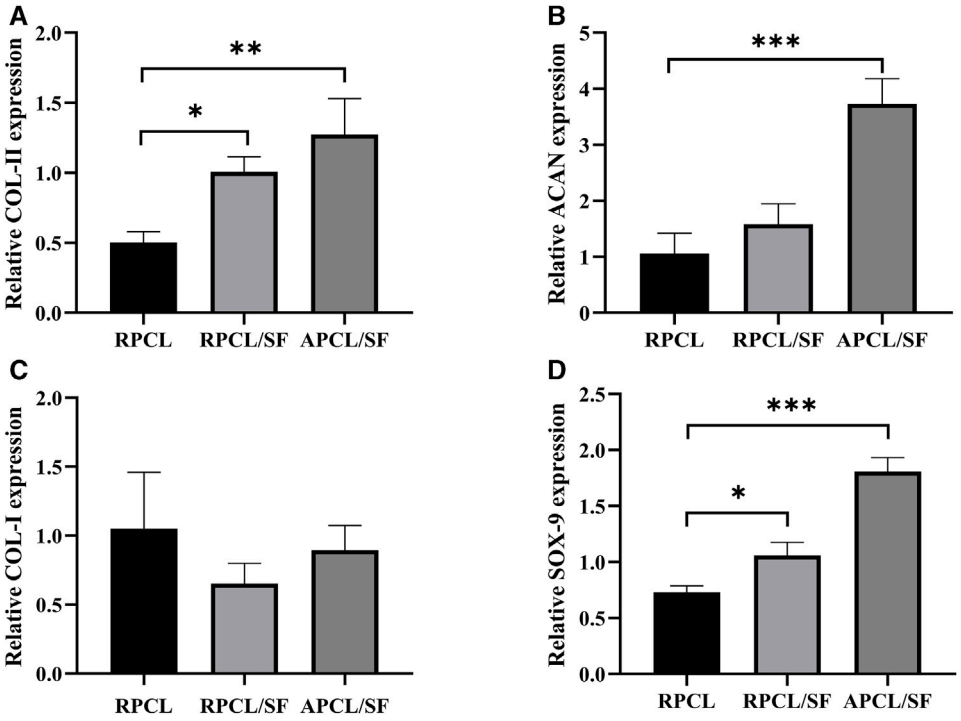

FIGURE 6
Expression of articular chondrocyte genes was analyzed for RPCL, RPCL/SF, and APCL/SF groups on day 7. **(A)** *COL-II* expression. **(B)** *ACAN* expression. **(C)** *COL-I* expression. **(D)** *SOX-9* expression. Comparison between the two groups, *$p < 0.05$, **$p < 0.01$, and ***$p < 0.001$.

nanofiber scaffolds increased on day 14, compared to day 7. This suggests that the scaffolds promoted cell growth and secretion of ECM by chondrocytes over time. Notably, the DNA contents and sGAG/DNA ratios in the APCL/SF group were significantly higher than those in the RPCL/SF and RPCL groups. Previous research suggests that cellular ECM secretion and differentiation are significantly impacted by material morphology, including chemical composition, wettability, and microstructure. Specifically, the presence of suitable surface pores on fibrous scaffolds is crucial for enhanced GAG formation, and effective GAG secretion implies deposition of cartilage matrix (Jonnalagadda et al., 2015; Ko et al., 2016).

Previous studies have shown that maintaining the chondrocyte phenotype is necessary in order to assess cartilage tissue repair *in vivo*, as substrate-producing cells in cartilage contribute to the formation of new tissue (Zhou et al., 2017). The expression of chondrocyte marker proteins, namely, *COL-II*, *ACAN*, *COL-I*, and *SOX-9*, is depicted in Figures 6A–D for the RPCL, RPCL/SF, and APCL/SF groups on day 7. The APCL/SF and RPCL/SF groups exhibited significantly elevated expression of the *SOX-9* and *COL-II* genes in comparison to RPCL group, and the differences were statistically significant. The *ACAN* gene expression was notably higher in the APCL/SF group than in the RPCL group with statistically significant differences, while no significant difference was found between the RPCL/SF and APCL/SF groups. No significant differences were observed in *COL-I* expression among the RPCL, RPCL/SF, and APCL/SF groups. Type II collagen is the principal structural element of articular cartilage in the ECM, and COL-II secretion increases with collagen maturation (Jacob et al., 2019). *SOX-9* regulates the expression of genes encoding type II collagen and proteoglycan aggregation proteins in the ECM. The increased expression of *SOX-9* in APCL/SF suggests its superior capacity to promote ECM secretion by chondrocytes (Song and Park, 2020). Importantly, the addition of SF to PCL led to a significantly greater increase in ECM secretion by RPCL/SF compared to RPCL. RPCL/SF increased *COL-II* gene expression more than RPCL, implying that SF facilitated chondrogenic gene expression. *Col-II* gene expression was notably greater in APCL/SF than in RPCL and RPCL/SF, indicating that the arrangement of nanofibers is a significant factor in stimulating Col-II secretion. Collagen synthesis may be higher in APCL/SF compared to RPCL and RPCL/SF.

Overall, the results of the *in vitro* experiment indicate that all of the three scaffolds effectively support the growth, proliferation and ECM secretion of articular chondrocytes. In particular, APCL/SF demonstrates better regeneration of articular chondrocytes. Consequently, the novel APCL/SF nanofiber scaffold presents a highly promising, xeno-free approach for regenerating articular cartilage. Future *in vivo* studies are necessary for assessing the regenerative capability of the APCL/SF nanofiber scaffold for treating articular cartilage defects in animal models.

4 Conclusion

This study employed the exceptional characteristics of PCL and SF to fabricate randomly oriented (RPCL and RPCL/SF) and aligned oriented (APCL/SF) nanofibrous scaffolds by electrospinning

technique. The effects of RPCL, RPCL/SF, and APCL/SF on chondrocyte regeneration were confirmed through material characterization tests and *in vitro* cellular responses. Compared to the RPCL and RPCL/SF scaffolds, the APCL/SF scaffold demonstrated enhanced mechanical properties and hydrophilicity that promote regeneration of articular cartilage. The scaffold significantly improved chondrocyte adhesion, growth, and alignment, as well as ECM secretion, and facilitated matrix deposition. These results suggest that the surface morphology of the material has an important effect on chondrocyte regeneration and the potential of the APCL/SF nanofiber scaffold for articular cartilage tissue regeneration.

Data availability statement

The raw data supporting the conclusion of this article will be made available by the authors, without undue reservation.

Ethics statement

The animal study was approved by the Animal Care and Use Committee of Beijing Keyu Animal Center (KY20230906002). The study was conducted in accordance with the local legislation and institutional requirements.

Author contributions

BX: Data curation, Formal Analysis, Investigation, Methodology, Visualization, Writing–original draft, Writing–review and editing. FY: Data curation, Formal Analysis, Investigation, Methodology, Visualization, Writing–original draft, Writing–review and editing. HC: Data curation, Formal Analysis, Investigation, Methodology, Visualization, Writing–original draft, Writing–review and editing. HZ: Data curation, Formal Analysis, Investigation, Methodology, Visualization, Writing–original draft, Writing–review and editing. HM: Methodology, Supervision, Validation, Writing–review and editing. TL: Methodology, Supervision, Validation, Writing–review and editing. ZC: Formal Analysis, Validation, Writing–review and editing. JL: Formal Analysis, Validation, Writing–review and editing. XL: Conceptualization, Funding acquisition, Methodology, Project administration, Supervision, Writing–review and editing. JD: Conceptualization, Funding acquisition, Methodology, Project administration, Supervision, Writing–review and editing.

Funding

The author(s) declare financial support was received for the research, authorship, and/or publication of this article. This work was supported by the Research Projects of Army Logistics Priority (BKJ20J004), the Promotion of Flying Personnel's Effectiveness (2019ZTA02), and the Top Young Talent Program (22BJQN006).

Conflict of interest

The authors declare that the research was conducted in the absence of any commercial or financial relationships that could be construed as a potential conflict of interest.

Publisher's note

All claims expressed in this article are solely those of the authors and do not necessarily represent those of their affiliated organizations, or those of the publisher, the editors and the reviewers. Any product that may be evaluated in this article, or claim that may be made by its manufacturer, is not guaranteed or endorsed by the publisher.

References

Armiento, A. R., Alini, M., and Stoddart, M. J. (2019). Articular fibrocartilage - why does hyaline cartilage fail to repair? *Adv. Drug Deliv. Rev.* 146, 289–305. doi:10.1016/j.addr.2018.12.015

Casanova, M. R., Reis, R. L., Martins, A., and Neves, N. M. (2018). The Use of electrospinning technique on osteochondral tissue engineering. *Adv Exp Med Biol.* 1058, 247–263. doi:10.1007/978-3-319-76711-6_11

Chen, C. H., Chen, S. H., Kuo, C. Y., Li, M. L., and Chen, J. P. (2017). Response of dermal fibroblasts to biochemical and physical cues in aligned polycaprolactone/silk fibroin nanofiber scaffolds for application in tendon tissue engineering. *Nanomater (Basel)* 7 (8), 219. doi:10.3390/nano7080219

Cheng, G., Chen, J., Wang, Q., Yang, X., Cheng, Y., Li, Z., et al. (2017). Promoting osteogenic differentiation in pre-osteoblasts and reducing tibial fracture healing time using functional nanofibers. *Nano Res.* 11, 3658–3677. doi:10.1007/s12274-017-1934-3

Christensen, B. B., Olesen, M. L., Hede, K. T. C., Bergholt, N. L., Foldager, C. B., and Lind, M. (2021). Particulated cartilage for chondral and osteochondral repair: a review. *Cartilage* 13 (1), 1047s–1057s. doi:10.1177/1947603520904757

Chung, J. Y., Youngblood, J. P., and Stafford, C. M. (2007). Anisotropic wetting on tunable micro-wrinkled surfaces. *Soft Matter* 3 (9), 1163–1169. doi:10.1039/b705112c

Critchley, S., Sheehy, E. J., Cunniffe, G., Diaz-Payno, P., Carroll, S. F., Jeon, O., et al. (2020). 3D printing of fibre-reinforced cartilaginous templates for the regeneration of osteochondral defects. *Acta Biomater.* 113, 130–143. doi:10.1016/j.actbio.2020.05.040

Farokhi, M., Mottaghitalab, F., Samani, S., Shokrgozar, M. A., Kundu, S. C., Reis, R. L., et al. (2018). Silk fibroin/hydroxyapatite composites for bone tissue engineering. *Biotechnol. Adv.* 36 (1), 68–91. doi:10.1016/j.biotechadv.2017.10.001

Faucheux, N., Schweiss, R., Lützow, K., Werner, C., and Groth, T. (2004). Self-assembled monolayers with different terminating groups as model substrates for cell adhesion studies. *Biomaterials* 25 (14), 2721–2730. doi:10.1016/j.biomaterials.2003.09.069

Gao, Y., Gao, J., Li, H., Du, D., Jin, D., Zheng, M., et al. (2019). Autologous costal chondral transplantation and costa-derived chondrocyte implantation: emerging surgical techniques. *Ther. Adv. Musculoskelet. Dis.* 11, 1759720X1987713. doi:10.1177/1759720x19877131

Guo, W., Chen, M., Wang, Z., Tian, Y., Zheng, J., Gao, S., et al. (2021). 3D-printed cell-free PCL–MECM scaffold with biomimetic micro-structure and micro-environment to enhance *in situ* meniscus regeneration. *Bioact. Mater.* 6 (10), 3620–3633. doi:10.1016/j.bioactmat.2021.02.019

Jacob, J., More, N., Mounika, C., Gondaliya, P., Kalia, K., and Kapusetti, G. (2019). Smart Piezoelectric Nanohybrid of poly(3-hydroxybutyrate-co-3-hydroxyvalerate) and barium Titanate for stimulated cartilage regeneration. *ACS Appl. Bio Mater* 2 (11), 4922–4931. doi:10.1021/acsabm.9b00667

Johnstone, B., Alini, M., Cucchiarini, M., Dodge, G. R., Eglin, D., Guilak, F., et al. (2013). Tissue engineering for articular cartilage repair--the state of the art. *Eur. Cell Mater* 25, 248–267. doi:10.22203/ecm.v025a18

Jonnalagadda, J. B., Rivero, I. V., and Dertien, J. S. (2015). *In vitro* chondrocyte behavior on porous biodegradable poly(e-caprolactone)/polyglycolic acid scaffolds for

articular chondrocyte adhesion and proliferation. *J. Biomater. Sci. Polym. Ed.* 26 (7), 401–419. doi:10.1080/09205063.2015.1015864

Jun, I., Han, H. S., Edwards, J. R., and Jeon, H. (2018). Electrospun fibrous scaffolds for tissue engineering: Viewpoints on Architecture and fabrication. *Int. J. Mol. Sci.* 19 (3), 745. doi:10.3390/ijms19030745

Kai, D., Prabhakaran, M., Jin, G., and Ramakrishna, S. (2011a). Guided orientation of cardiomyocytes on electrospun aligned nanofibers for cardiac tissue engineering. *J. Biomed. Mater. Res. Part B, Appl. biomaterials* 98B, 379–386. doi:10.1002/jbm.b.31862

Kai, D., Prabhakaran, M. P., Jin, G., and Ramakrishna, S. (2011b). Guided orientation of cardiomyocytes on electrospun aligned nanofibers for cardiac tissue engineering. *J. Biomed. Mater Res. B Appl. Biomater.* 98 (2), 379–386. doi:10.1002/jbm.b.31862

Ki, C., Park, Y. H., and Jin, H.-J. (2009). Silk protein as a Fascinating biomedical polymer: structural Fundamentals and applications. *Macromol. Res.* 17, 935–942. doi:10.1007/BF03218639

Ko, C. Y., Ku, K. L., Yang, S. R., Lin, T. Y., Peng, S., Peng, Y. S., et al. (2016). *In vitro* and *in vivo* co-culture of chondrocytes and bone marrow stem cells in photocrosslinked PCL-PEG-PCL hydrogels enhances cartilage formation. *J. Tissue Eng. Regen. Med.* 10 (10), E485–e496. doi:10.1002/term.1846

Lampin, M., Warocquier, C., Legris, C., Degrange, M., and Sigot-Luizard, M. F. (1997). Correlation between substratum roughness and wettability, cell adhesion, and cell migration. *J. Biomed. Mater Res.* 36(1), 99–108. doi:10.1002/(sici)1097-4636(199707)36:1<99::aid-jbm12>3.0.co;2-e

Lee, H., and Kim, G. (2010). Biocomposites electrospun with poly(ε-caprolactone) and silk fibroin powder for biomedical applications. *J. Biomater. Sci. Polym. Ed.* 21 (13), 1687–1699. doi:10.1163/092050609x12548956645680

Lee, H., Yeo, M., Ahn, S., Kang, D. O., Jang, C. H., Lee, H., et al. (2011). Designed hybrid scaffolds consisting of polycaprolactone microstrands and electrospun collagen-nanofibers for bone tissue regeneration. *J. Biomed. Mater Res. B Appl. Biomater.* 97 (2), 263–270. doi:10.1002/jbm.b.31809

Li, G., Li, Y., Chen, G., He, J., Han, Y., Wang, X., et al. (2015). Silk-based biomaterials in biomedical textiles and fiber-based implants. *Adv. Healthc. Mater* 4 (8), 1134–1151. doi:10.1002/adhm.201500002

Li, L., Li, H., Qian, Y., Li, X., Singh, G. K., Zhong, L., et al. (2011). Electrospun poly (ε-caprolactone)/silk fibroin core-sheath nanofibers and their potential applications in tissue engineering and drug release. *Int. J. Biol. Macromol.* 49 (2), 223–232. doi:10.1016/j.ijbiomac.2011.04.018

Li, Z., Liu, P., Yang, T., Sun, Y., You, Q., Li, J., et al. (2016). Composite poly(l-lactic-acid)/silk fibroin scaffold prepared by electrospinning promotes chondrogenesis for cartilage tissue engineering. *J. Biomater. Appl.* 30 (10), 1552–1565. doi:10.1177/0885328216638587

Liao, G., Jiang, S., Xu, X., and Ke, Y. (2012). Electrospun aligned PLLA/PCL/HA composite fibrous membranes and their *in vitro* degradation behaviors. *Mater. Lett.* 82, 159–162. doi:10.1016/j.matlet.2012.05.085

Lowery, J. L., Datta, N., and Rutledge, G. C. (2010). Effect of fiber diameter, pore size and seeding method on growth of human dermal fibroblasts in electrospun poly(ε-caprolactone) fibrous mats. *Biomaterials* 31 (3), 491–504. doi:10.1016/j.biomaterials.2009.09.072

Makris, E. A., Gomoll, A. H., Malizos, K. N., Hu, J. C., and Athanasiou, K. A. (2015). Repair and tissue engineering techniques for articular cartilage. *Nat. Rev. Rheumatol.* 11 (1), 21–34. doi:10.1038/nrrheum.2014.157

Malikmammadov, E., Tanir, T. E., Kiziltay, A., Hasirci, V., and Hasirci, N. (2018). PCL and PCL-based materials in biomedical applications. *J. Biomater. Sci. Polym. Ed.* 29 (7-9), 863–893. doi:10.1080/09205063.2017.1394711

Min, B. M., Lee, G., Kim, S. H., Nam, Y. S., Lee, T. S., and Park, W. H. (2004). Electrospinning of silk fibroin nanofibers and its effect on the adhesion and spreading of normal human keratinocytes and fibroblasts *in vitro*. *Biomaterials* 25 (7-8), 1289–1297. doi:10.1016/j.biomaterials.2003.08.045

Na, Y., Shi, Y., Liu, W., Jia, Y., Kong, L., Zhang, T., et al. (2019). Is implantation of autologous chondrocytes superior to microfracture for articular-cartilage defects of the knee? A systematic review of 5-year follow-up data. *Int. J. Surg.* 68, 56–62. doi:10.1016/j.ijsu.2019.06.007

Orash Mahmoud Salehi, A., Nourbakhsh, M. S., Rafienia, M., Baradaran-Rafii, A., and Heidari Keshel, S. (2020). Corneal stromal regeneration by hybrid oriented poly (ε-caprolactone)/lyophilized silk fibroin electrospun scaffold. *Int. J. Biol. Macromol.* 161, 377–388. doi:10.1016/j.ijbiomac.2020.06.045

Qin, Z., He, Y., Gao, J., Dong, Z., Long, S., Cheng, L., et al. (2023). Surface modification improving the biological activity and osteogenic ability of 3D printing porous dental implants. *Front. Mater.* 10. doi:10.3389/fmats.2023.1183902

Redondo, M. L., Beer, A. J., and Yanke, A. B. (2018). Cartilage Restoration: microfracture and osteochondral Autograft transplantation. *J. Knee Surg.* 31 (3), 231–238. doi:10.1055/s-0037-1618592

Rockwood, D. N., Preda, R. C., Yücel, T., Wang, X., Lovett, M. L., and Kaplan, D. L. (2011). Materials fabrication from Bombyx mori silk fibroin. *Nat. Protoc.* 6 (10), 1612–1631. doi:10.1038/nprot.2011.379

Roy, T., Maity, P. P., Rameshbabu, A. P., Das, B., John, A., Dutta, A., et al. (2018). Core-Shell nanofibrous scaffold based on polycaprolactone-silk fibroin Emulsion electrospinning for tissue engineering applications. *Bioeng. (Basel)* 5 (3), 68. doi:10.3390/bioengineering5030068

Sahoo, S., Toh, S. L., and Goh, J. C. (2010). A bFGF-releasing silk/PLGA-based biohybrid scaffold for ligament/tendon tissue engineering using mesenchymal progenitor cells. *Biomaterials* 31 (11), 2990–2998. doi:10.1016/j.biomaterials.2010.01.004

Saracino, E., Cirillo, V., Marrese, M., Guarino, V., Benfenati, V., Zamboni, R., et al. (2021). Structural and functional properties of astrocytes on PCL based electrospun fibres. *Mater Sci. Eng. C Mater Biol. Appl.* 118, 111363. doi:10.1016/j.msec.2020.111363

Saremi, J., Khanmohammadi, M., Azami, M., Ai, J., Yousefi-Ahmadipour, A., and Ebrahimi-Barough, S. (2021). Tissue-engineered nerve graft using silk-fibroin/polycaprolactone fibrous mats decorated with bioactive cerium oxide nanoparticles. *J. Biomed. Mater Res. A* 109 (9), 1588–1599. doi:10.1002/jbm.a.37153

Schmittgen, T. D., and Livak, K. J. (2008). Analyzing real-time PCR data by the comparative C(T) method. *Nat. Protoc.* 3 (6), 1101–1108. doi:10.1038/nprot.2008.73

Silva, J. C., Udangawa, R. N., Chen, J., Mancinelli, C. D., Garrudo, F. F. F., Mikael, P. E., et al. (2020). Kartogenin-loaded coaxial PGS/PCL aligned nanofibers for cartilage tissue engineering. *Mater Sci. Eng. C Mater Biol. Appl.* 107, 110291. doi:10.1016/j.msec.2019.110291

Song, H., and Park, K. H. (2020). Regulation and function of SOX9 during cartilage development and regeneration. *Semin. Cancer Biol.* 67 (1), 12–23. doi:10.1016/j.semcancer.2020.04.008

Steffi, C., Wang, D., Kong, C. H., Wang, Z., Lim, P. N., Shi, Z., et al. (2018). Estradiol-Loaded poly(ε-caprolactone)/silk fibroin electrospun Microfibers decrease Osteoclast activity and Retain osteoblast function. *ACS Appl. Mater Interfaces* 10 (12), 9988–9998. doi:10.1021/acsami.8b01855

Teh, T. K., Toh, S. L., and Goh, J. C. (2010). Optimization of the silk scaffold sericin removal process for retention of silk fibroin protein structure and mechanical properties. *Biomed. Mater* 5 (3), 035008. doi:10.1088/1748-6041/5/3/035008

Torricelli, P., Gioffrè, M., Fiorani, A., Panzavolta, S., Gualandi, C., Fini, M., et al. (2014). Co-electrospun gelatin-poly(L-lactic acid) scaffolds: modulation of mechanical properties and chondrocyte response as a function of composition. *Mater Sci. Eng. C Mater Biol. Appl.* 36, 130–138. doi:10.1016/j.msec.2013.11.050

Wang, Z., Song, X., Cui, Y., Cheng, K., Tian, X., Dong, M., et al. (2021). Silk fibroin H-fibroin/poly(ε-caprolactone) core-shell nanofibers with enhanced mechanical property and long-term drug release. *J. Colloid Interface Sci.* 593, 142–151. doi:10.1016/j.jcis.2021.02.099

Xie, X., Yu, J., Zhao, Z., Zheng, Z., Xie, M., Wang, X., et al. (2019). Fabrication and drug release properties of curcumin-loaded silk fibroin nanofibrous membranes. *Adsorpt. Sci. Technol.* 37 (5-6), 412–424. doi:10.1177/0263617418820416

Xue, J., Qin, C., and Wu, C. (2023). 3D printing of cell-delivery scaffolds for tissue regeneration. *Regen. Biomater.* 10, rbad032. doi:10.1093/rb/rbad032

Yang, J., Wang, H., Zhou, Y., Duan, L., Schneider, K. H., Zheng, Z., et al. (2023). Silk fibroin/Wool Keratin composite scaffold with Hierarchical fibrous and porous structure. *Macromol. Biosci.* 23 (10), e2300105. doi:10.1002/mabi.202300105

Yuan, H., Shi, H., Qiu, X., and Chen, Y. (2016). Mechanical property and biological performance of electrospun silk fibroin-polycaprolactone scaffolds with aligned fibers. *J. Biomater. Sci. Polym. Ed.* 27 (3), 263–275. doi:10.1080/09205063.2015.1120475

Zelinka, A., Roelofs, A. J., Kandel, R. A., and De Bari, C. (2022). Cellular therapy and tissue engineering for cartilage repair. *Osteoarthr. Cartil.* 30 (12), 1547–1560. doi:10.1016/j.joca.2022.07.012

Zhang, X., Reagan, M. R., and Kaplan, D. L. (2009). Electrospun silk biomaterial scaffolds for regenerative medicine. *Adv. Drug Deliv. Rev.* 61 (12), 988–1006. doi:10.1016/j.addr.2009.07.005

Zhang, Y., Yang, F., Liu, K., Shen, H., Zhu, Y., Zhang, W., et al. (2012). The impact of PLGA scaffold orientation on *in vitro* cartilage regeneration. *Biomaterials* 33 (10), 2926–2935. doi:10.1016/j.biomaterials.2012.01.006

Zhao, W., Du, Z., Fang, J., Fu, L., Zhang, X., Cai, Q., et al. (2020). Synthetic/natural blended polymer fibrous meshes composed of polylactide, gelatin and glycosaminoglycan for cartilage repair. *J. Biomater. Sci. Polym. Ed.* 31 (11), 1437–1456. doi:10.1080/09205063.2020.1760701

Zhou, F., Zhang, X., Cai, D., Li, J., Mu, Q., Zhang, W., et al. (2017). Silk fibroin-chondroitin sulfate scaffold with immuno-inhibition property for articular cartilage repair. *Acta Biomater.* 63, 64–75. doi:10.1016/j.actbio.2017.09.005

Zhou, Y., Chyu, J., and Zumwalt, M. (2018). Recent progress of fabrication of cell scaffold by electrospinning technique for articular cartilage tissue engineering. *Int. J. Biomater.* 2018, 1–10. doi:10.1155/2018/1953636

Zhou, Z., Zheng, J., Meng, X., and Wang, F. (2023). Effects of electrical stimulation on articular cartilage regeneration with a focus on Piezoelectric biomaterials for articular cartilage tissue repair and engineering. *Int. J. Mol. Sci.* 24 (3), 1836. doi:10.3390/ijms24031836